# Research Plan

for a Doctoral Study in Physics at the D-PHYS of ETH Zurich

Laura Paulina Šinkūnaitė

## 1 Introduction and motivation

**Proton radius puzzle** The previously conducted measurements [4] of the $2S - 2P$ energy splitting in muonic hydrogen ($\mu p$) from the triplet ($2S^{F=1}_{1/2} - 2P^{F=2}_{3/2}$) and the singlet ($2S^{F=0}_{1/2} - 2P^{F=1}_{3/2}$) $2S$ sub-levels has shown a $7\sigma$ discrepancy comparing to the values extracted from the electron-proton scattering and hydrogen ($H$) spectroscopy. This so-called "proton radius puzzle" is interesting for different areas of physics research: the reanalysis of electron-proton scattering data, verifications of the proton structure at low energies, new determinations of the Rydberg constant, and new scattering experiments with electrons and muons. So far, the resolution of the "proton radius puzzle" remains unknown.

**Hyperfine splitting** A new experiment (HyperMu) designed to contribute to the resolution of the "proton radius puzzle" is being developed at the Paul Scherrer Institute (PSI). HyperMu is aiming to measure the ground-state hyperfine splitting ($1S - HFS$) in $\mu p$ and in muonic helium ($\mu^3 He^+$) with an accuracy of 1 ppm by means of laser spectroscopy. From the successful measurement of the $1S - HFS$ transition, the corresponding nuclear-structure - related effects can be determined with a relative accuracy of $1 \times 10^{-4}$. These effects arise from the two-photon exchange (TPE) process (Figure 1).

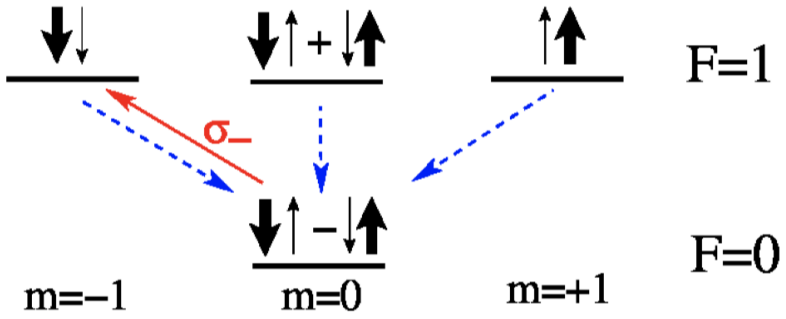


Figure 1: Energy levels and spin compositions of the $1S$ states in $\mu p$. The red arrow represents the transition driven by the circularly polarised laser light, the blue arrows illustrate the collisional quenching [1].

**Two-photon exchange** The TPE can be divided into an elastic part, i.e. Zemach radius contribution, and an inelastic part, i.e. polarisability contribution.

$$\Delta TPE = \Delta z + \Delta_{recoil} + \Delta_{pol}, \tag{1}$$

where the elastic Zemach contribution is

$$\Delta z = \frac{8Z\alpha m_r}{\pi}\int_0^\infty \frac{dQ}{Q^2}\left(G_E(Q^2)\frac{G_M(Q^2)}{1+\kappa_p} - 1\right) = -2(Z\alpha)m_r R_Z, \tag{2}$$

where the inelastic Zemach radius is defined as

$$R_Z = -\frac{4}{\pi}\int_0^\infty \frac{dQ}{Q^2}\left(G_E(Q^2)\frac{G_M(Q^2)}{1+\kappa_p} - 1\right), \tag{3}$$

where $\kappa_p$ is a term related to the dipole magnetic moment of the proton. This non-relativistically reduces to the convolution of charge and magnetic distributions

$$R_Z = \int d^3\boldsymbol{r}|\boldsymbol{r}|\int d^3\boldsymbol{r'}\rho_E(\boldsymbol{r}-\boldsymbol{r'})\rho_M(\boldsymbol{r'}). \tag{4}$$

This is the contribution with the largest uncertainty of the order of $1\times10^{-4}$. The mixed finite-size recoil correction term to the Zemach term,

$$\Delta_{recoil} \sim 2\times10^{-3}, \tag{5}$$

can be expressed as an integral over $Q^2$ of the Sachs Form Factors, $G_E(Q^2)$ and $G_M(Q^2)$, and of the proton structure functions, $F_1(Q^2)$, and $F_2(Q^2)$. There are two approaches to evaluate the TPE contribution: using dispersion relations and data such as structure functions and form factors or using chiral perturbation theory. In a dispersive approach, the inelastic contribution can be fully calculated using the spin-dependent structure functions of the proton, $g_1(x, Q^2)$ and $g_2(x, Q^2)$ [1].

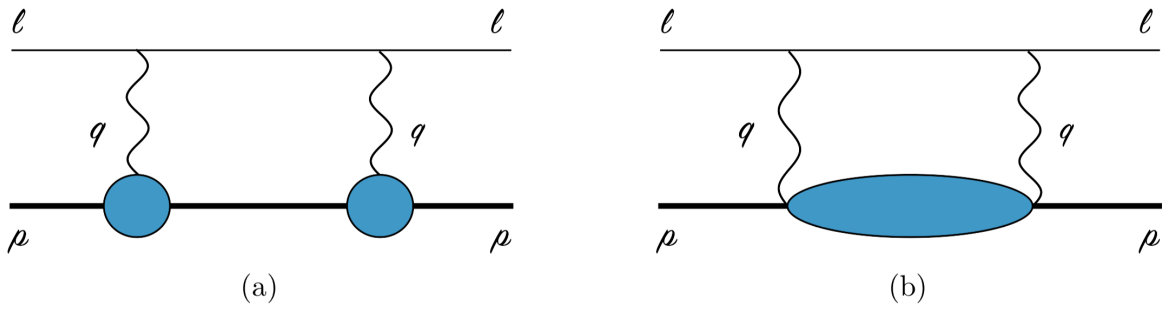


Figure 2: TPE diagrams in forward kinematics: the horizontal lines correspond to the lepton and the nucleus (bold). (a) Elastic contribution to the TPE diagram. (b) Inelastic contribution to the TPE diagram, where the "blob" represents all possible excitations [3].

**Motivation** The precise measurement of the $1S - HFS$ transition in the $\mu p$ to evaluate the TPE contribution would increase our understanding of the low-energy structure of the proton and would provide a benchmark for chiral perturbation theory, dispersion-based approaches, and lattice QCD. It would also be a test of the lepton universality, i.e. when $\mu p$ laser spectroscopy results are compared to the electron-proton scattering and to the electronic hydrogen ($ep$) spectroscopy, and on top of that it would impact the resolution of the "proton radius puzzle" and the related "new physics" searches.

# 2 Working principle

**The principle of the HyperMu experiment:** A muon is stopped in hydrogen gas forming a $\mu p$ atom in a highly-excited state. The formed $\mu p$ atom de-excites to the $F = 0$ sub-level of the ground state. A high-energy laser pulse ($3$ mJ at $6.7\mu m$ and at $500$ Hz repetition rate) excites the $\mu p$ atom,

$$\mu p_{F=0} + \gamma \rightarrow \mu p_{F=1}.$$

In a collision with a hydrogen molecule ($H_2$), the $\mu p$ atom is de-excited to the $F = 0$ sub-level of the ground state and after $\sim 1\ \mu s$ is thermalised to the hydrogen gas temperature ($50$ K),

$$\mu p_{F=1} + H_2 \rightarrow \mu p_{F=0} + H_2 + E_{kin}.$$

This transition energy is converted into the kinetic energy. Having this extra kinetic energy, the $\mu p$ atom efficiently diffuses to the target walls before muon decay occurs. At the target wall, which is made of the high-Z material, the muon is transferred from the $\mu p$ to the high-Z material forming $(\mu Z)^*$ in an excited state. The highly-excited $(\mu Z)^*$ atoms then de-excite producing MeV X-rays. The MeV X-rays are detected using scintillating detectors (Figure 2). A resonance curve is obtained by plotting the number of the X-rays versus the laser frequency.

**Signature of an event** The signal events are considered to be the MeV X-rays detected within a time window $\Delta t$ after the laser excitation. There are two types of background events: intrinsic and erroneous. The intrinsic background is produced by non-laser excited $\mu p$ atoms, that diffuse to the target walls in the observation time window $\Delta t$. This type of background can be minimised by cooling down the target, e.g. keeping the $H_2$ gas at $50$ K temperature. The other type of background arises from the electrons produced in the event of a muon decay and being falsely identified as the X-rays.

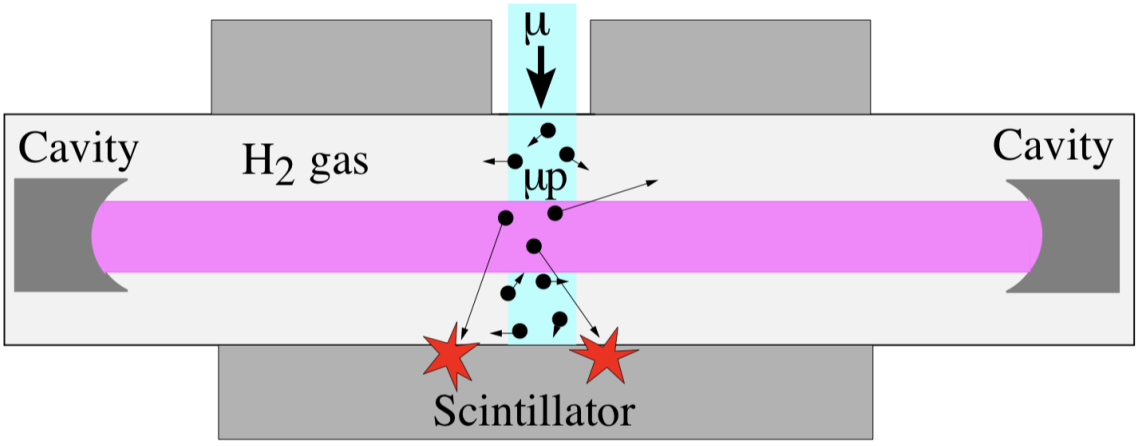


Figure 3: Preliminary HyperMu experimental scheme showing a laser cavity, muon entrance beam, and the surrounding scintillating detectors [1].

**Laser system** To produce a resonance curve for the $1S - HFS$ transition in the $\mu p$, a high-energy (3 mJ), spectroscopy-quality pulsed laser is needed. There are two ways to approach this wavelength: by using a Ti:Sa laser and a Raman cell or by using a sequence of non-linear crystals in OPO and OPA technologies. The first scheme is similar as used in 2009 for the $2S - 2P$ measurement in the $\mu p$ but with an increased performance by an order of magnitude. A pulse energy of 3 mJ at $6.7\mu$m would be needed for the HFS. The laser system would be composed by a thin-disk laser followed by a pulsed Ti:Sa laser seeded by a continuous wave (cw) frequency stabilised laser at a wavelength of about 730 nm. The $6.7\mu$m wavelength would be reached using 3 Stokes shifts in a $H_2$ Raman cell [1]. However, this scheme has rather limited pulse energy and repetition rate due to the heating effects. Therefore, the Raman cell is being planned to be replaced with parametric down-conversion stages based on the non-linear crystals in OPO and OPA technologies [2]. Using this OPO and OPA scheme, the thin-disk laser would be operated in single-frequency mode achieved by injection seeding the thin-disk laser oscillator with an external frequency stabilised cw laser at 1030 nm. The pulses at 1030 nm

would then be down-converted in a non-linear crystal to produce two beams, so called an "idler" beam at $2434$ nm and a "signal" beam at $1785$ nm. The OPO cavity would then be seeded by a tunable "signal" laser used to scan the resonance. A successive difference frequency generation (DFG) between "idler" and "signal" pulses would then be used to generate $3$ mJ pulses at $6.7\mu$m (Figure 2).

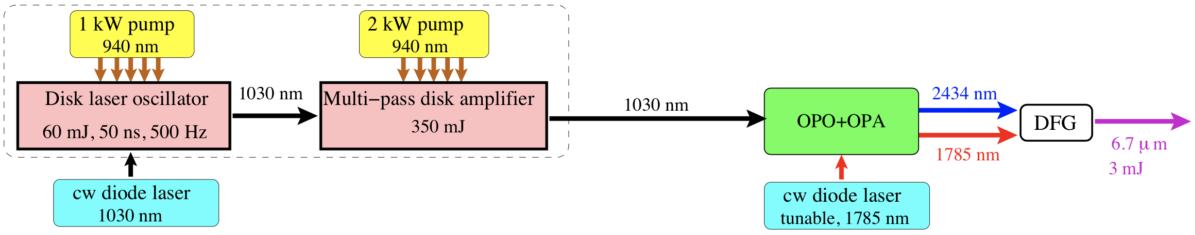


Figure 4: Possible parametric down-conversion laser scheme for $\mu p$ experiment using new OPO and OPA technologies [1].

# 3 Research activities / Interim results

**HypereX detector** The first part of the PhD candidate's work will be concentrated on the development and optimisation of the detection system (HypereX) for the HyperMu experiment. As considered above, the detector system not only needs to be able to detect MeV X-ray signal, but also to reject the erroneous background events caused by the electrons coming from the muon decay. Thus, to conquer this problem, different scintillating detector geometries and materials are being considered using a Monte Carlo simulation package $G4Beamline$, with the two emerging schemes that look quite promising.

**Cylindrical detector in a magnetic field** One detection scheme is employing the usage of a homogeneous $5$ T magnetic field surrounding the target and the detection regions. This would make charged particles spiral along the beam axis and would not allow them to deposit any energy in the cylindrical detector surrounding the beam axis. Thus, the false-identification of the negatively charged electrons would be minimised and the detection of the X-rays would be increased as they would scatter off the target walls and would deposit some energy in the cylindrical detector due to the solid angle. Even though, this scheme could provide us with a better beam intensity, good falsely-identified background rejection and a necessary X-ray detection efficiency, it would also cause us some challenges. Some of them would be lack of space for the optical cavity, harder access of the detectors and the experimental mechanics, and finally, increased costs and duration for the magnet's manufacture.

**Detector with a planar geometry** Another detection scheme would introduce a simple planar geometry, i.e. slabs of the scintillating materials of different thicknesses positioned around the target region with respect to the solid angle. This scheme would also use the pre-study of the different behaviour of the X-rays and of the electrons when traversing the material. The

electrons deposit energy continuously, at an almost constant $\sim 2MeV/cm$ rate in a light plastic scintillating detector, whereas the X-rays deposit energy in bunches in a more abrupter manner. Knowing these differences, a variation of the detectors and different energy thresholds can be used, e.g. making a sandwich detector. Thus, this feature relating the detector's thickness versus the amount of the deposited energy is being elaborated in this second scheme.

**Advanced considerations** Sticking with the planar geometry, more considerations are being tested using the $G4Beamline$ simulations. This includes changing the transverse and lateral size of the detectors, which shows some immediate effects: the thicker the detector is, the more likely that an X-ray will deposit some energy in it, the wider it is, the bigger solid angle it covers and the more hits of the scattering off particles it detects. Depending on the placement of the detectors, i.e. if we have symmetric detectors positioned in the up-stream and in the down-stream directions, we car harness the use of the multiplicities. That means, that a background event coming from a muon decay would have a more preferable directions, whereas an event coming from an X-ray cascade would scatter off and would deposit energy more isotropically. Moving the detectors away from the optical cavity, i.e. introducing a z-shift, and changing the diameter of the mechanics surrounding the target, i.e. introducing a $\phi$-shift, also shows some significant differences (Figures 3 and 5).

**Further development** As can be seen from the above, the parameters that can be redeveloped and optimised are endless. The next step is to introduce the missing physical processed into the simulation package, i.e. nuclear capture and muon transfer to gold). After re-optimisation of the already considered parameters and after reaching a high enough X-ray detection efficiency and a low enough electron misidentification as an X-ray probability in the simulations, a design will be established for the manufacture. One of the beam times will be used to test this design.

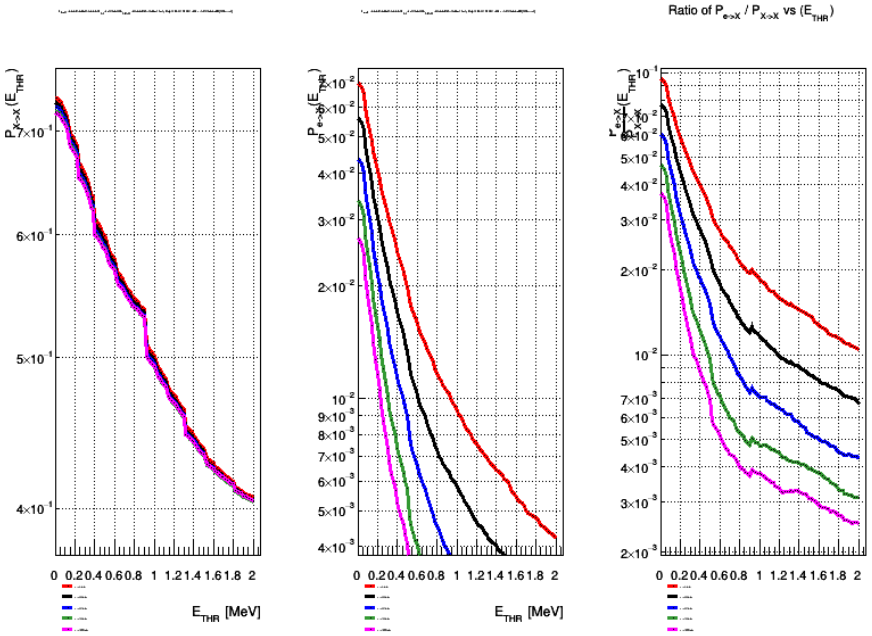


Figure 5: Comparison of the $phi$ shifts: 0-, 25-, 50-, 75-, and 100-mm. Obtained keeping the $z$-shift constant, Keeping no shift in the $z$-direction, i.e. $z = 0$-mm, and varying the $phi$ between 0-, 25-, 50-, 75-, and 100-mm.

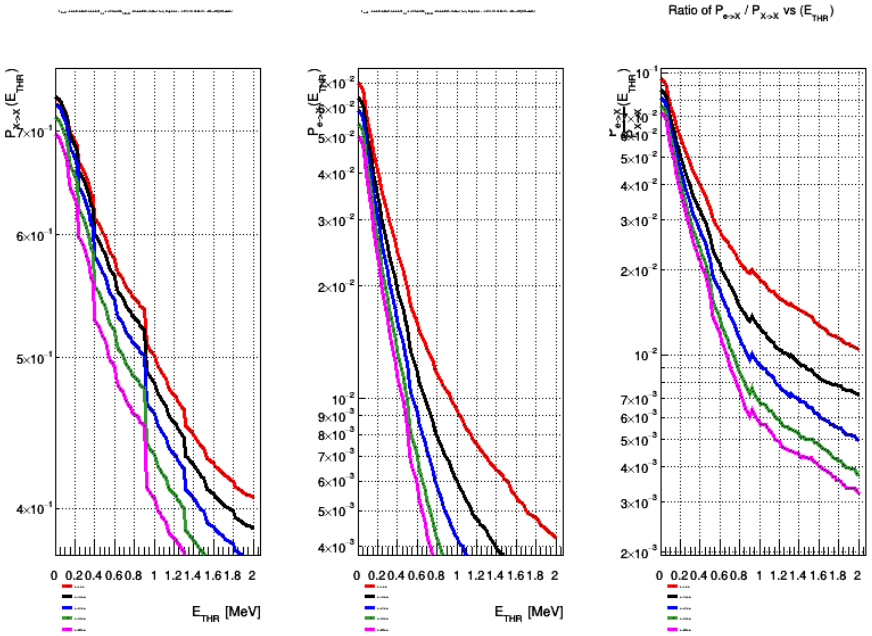


Figure 6: Comparison of the $phi$ shifts: 0-, 25-, 50-, 75-, and 100-mm. Obtained keeping the $z$-shift constant, Keeping no shift in the $z$-direction, i.e. $z = 0$-mm, and varying the $phi$ between 0-, 25-, 50-, 75-, and 100-mm.

# 4 Schedule of the research work

**2017 (done)**

- Initial detector simulations:
  - Geometry, various materials, costs.
- Observation of the development of the single-frequency external cavity tapered amplifier laser system by the researchers from the National Tsing Hua University in Taiwan.

**2018 (partially done)**

- Further detector simulations:
  - Geometry, various wall materials, detector materials; consider costs; include nuclear capture processes.
  - Study off-line response of the detector efficiencies, multiplicities.
  - Event analysis, X-ray nuclear capture signal, electron ($e^-$) signal.
- Initial analysis of the beam aspects (continuation of work conducted by Felix Berg):
  - Familiarisation of the Felix's simulations.

**2019**

- Initial analysis of the beam aspects (continuation of work conducted by Felix Berg):
  - Simulation of the beam line to see if we can improve the size of the beam.
  - Study the $\mu^-$ beam when focused with a small solenoid.
  - Simulation of an alternative beam-line in $\pi e5$.
- 2 test beam times:

- Preparation for the beam-time.
- Test the detection system.
- Test diffusion processes at various temperatures to validate Jonas Nuber's simulations.
- Test the rejection of the background.
- Measure stopping efficiencies.
- Analysis of the data from the 2017 test-run.
- Set-up of the data acquisition (DAQ) system.

- Working on Optical Parametric Oscillator (OPO), Optical Parametric Amplifier (OPA), and Double-Frequency Generator (DFG):
  - Check the various schemes and various crystal materials.
  - Simulation of the scheme and its optimisation.
  - Test the scheme in the laboratory.
  - Characterisation of the pulse output.
  - Spectroscopy of the absorption lines.

**2020**

- Development of the global settings:
  - Development and installation of the data acquisition (DAQ) system.
  - Target finalisation and installation.
  - Detector finalisation and installation.
  - Laser system's finalisation and installation.
- Beam-time, Physics run.

- Analysis of the beam-time data.

**2021**

- Analysis of the beam-time data.
- Writing of the thesis.

# 5 Teaching activities

Previous teaching duties were:

- 2018 - Teaching assistant for General Physics 2 (FS, Prof. K. Kirch)
- 2018 - Proton Irradiation Facility (PIF) shift operator (HS, Dr. W. Hajdas)

Further activities are planned at the PIF at PSI and should occupy $10 - 13\%$ of the total workload, as needed.

# References


[1] The CREMA collaboration. *Proposal for an experiment at PSI: Hyperfine splittings in muonic hydrogen and 3He.* 2016.

[2] Xiaobing Xie et al. *Injection-seeded single frequency* $2.05\ \mu m$ *output by ring cavity optical parametric oscillator*. Chinese Optics Letters, **15**(9), 2017.

[3] Franziska Hagelstein. *PhD thesis: Exciting nucleons in Compton scattering and hydrogen-like atoms.* arXiv: 1710.00874v1, 2017.

[4] The CREMA collaboration. *Laser Spectroscopy of Muonic Atoms and Ions.* arXiv: 1609.03440v1, 2016.

[5] Aldo Antognini, Franz Kottmann, François Biraben, Paul Indelicato, François Nez, and Randolf Pohl. *Theory of the* $2S - 2P$ *Lamb shift and* $2S$ *hyperfine splitting in muonic hydrogen.* arXiv: 1208.2637v2, 2012.